A general precipitation strategy for large-scale synthesis of molybdate nanostructures†

Cheng Peng, Lian Gao,* Songwang Yang and Jing Sun

Received (in Cambridge, UK) 14th July 2008, Accepted 19th August 2008
First published as an Advance Article on the web 25th September 2008
DOI: 10.1039/b812033a

A general precipitation strategy has been developed for the large-scale synthesis of molybdate nanostructures, and a series of molybdate nanostructures such as $Fe_2(MoO_4)_3$ nanoparticles, $ZnMoO_4$ nanoplates, $MnMoO_4$ nanorods and $CoMoO_4$ nanowires have been successfully prepared.

Recently, the morphology- and size-dependent properties of nanostructured materials have made the controlled synthesis of oxide nanostructures a continuously active field.[1] As a fascinating group of inorganic-functional materials, ternary metal oxides usually exhibit unique chemical and physical properties distinct from binary oxides.[2] Consequently, ternary metal oxide systems such as ferrites, tungstates and molybdates, have been extensively investigated in the past several decades. In particular, molybdates have attracted special attention because of their wide use not only as catalysts,[3] luminescence materials,[4] inhibitive pigments,[5] but also as promising candidate materials for electrodes in lithium ion batteries.[6] Molybdates are also attractive due to their semiconducting properties.[7] However, investigations on nanostructured molybdates are highly limited because the complex nature of molybdates makes the synthesis of nanostructures difficult. Thus, developing a simple pathway to synthesize molybdate nanostructures is of urgent significance for the further development of molybdates.

Conventionally, molybdates were prepared by the solid state reaction of MoO_3 with other metal oxides,[6a,8] but the high reaction temperature required usually resulted in grain growth, which was deleterious to nanostructures. Molybdates were also prepared by a precipitation heat-treatment method. The precipitation needed to be carefully controlled at 85 °C, otherwise the non-stoichiometric precursor was obtained.[3a] Recently, some new methods were utilized to synthesize nanostructured molybdates, such as the hydrothermal method,[9] complex precursor routes[10] and other routes.[7b,11] However, it still remains a challenge to synthesize molybdate nanostructures on the large-scale under a facile and environment-friendly condition.

State Key Lab of High Performance Ceramics and Superfine Microstructure, Shanghai Institute of Ceramics, Chinese Academy of Sciences, Shanghai, 200050, P. R. China.
E-mail: liangaoc@online.sh.cn; Fax: +86-21-52413122; Tel: +86-21-52412718

† Electronic supplementary information (ESI) available: Characterization; thermal behavior of $ZnMoO_4{\cdot}nH_2O$; additional SEM and TEM images. See DOI: 10.1039/b812033a

In this paper, we report a general precipitation strategy for the large-scale synthesis of molybdate nanostructures. A series of molybdate nanostructures such as $Fe_2(MoO_4)_3$ nanoparticles, $ZnMoO_4$ nanoplates , $MnMoO_4$ nanorods and $CoMoO_4$ nanowires has been successfully synthesized. With nitrates and ammonium heptamolybdate as starting materials, this method is based on a room temperature precipitation and a subsequent 400 °C heat-treatment. Compared with the above mentioned methods, the method is easy and independent of harsh reaction conditions or expensive organic solvents, and thus provides us a facile, low-cost and environment-friendly route for the large-scale synthesis of molybdate nanostructures.

Analytical pure nitrates and ammonium heptamolybdate were used as obtained. In a typical synthesis of $ZnMoO_4$ nanoplates, $(NH_4)_6Mo_7O_{24}{\cdot}4H_2O$ (2 mmol) was dissolved in deionized water (200 mL) completely. $NH_3{\cdot}H_2O$ (8–12 mL, 2 mol L^{-1}) was added to form a mixed solution. Under vigorous agitation, an aqueous solution (100 mL) containing $Zn(NO_3)_2{\cdot}6H_2O$ (14 mmol, the mole ratio of Mo to metal, R_m is 1.0) was slowly dropped into the above solution at room temperature. After stirring for 2 h, the precipitate was filtered, washed with deionized water and absolute ethanol and dried at 50 °C for 5 h. White $ZnMoO_4$ powders were obtained by a subsequent 400 °C heat-treatment of the precipitation. When $Zn(NO_3)_2{\cdot}6H_2O$ was replaced by $Fe(NO_3)_3{\cdot}9H_2O$ (9.3 mmol, R_m is 1.5), $Mn(NO_3)_2$ (14 mmol, R_m is 1.0), $Co(NO_3)_2{\cdot}6H_2O$ (14 mmol, R_m is 1.0), $Fe_2(MoO_4)_3$, $MnMoO_4$ and $CoMoO_4$ were obtained by performing the same precipitation heat-treatment procedures, respectively.

The crystal structures of all the samples were examined by X-ray diffraction (XRD) and the results are shown in Fig. 1. The diffraction peaks in Fig. 1a can be indexed to the monoclinic $Fe_2(MoO_4)_3$ phase (JCPDS No. 83-1701). When zinc nitrate is used as a starting material, triclinic $ZnMoO_4$ (JCPDS No. 35-0765) is obtained (Fig. 1b). Manganese nitrate leads to the formation of monoclinic $MnMoO_4$ (JCPDS No. 72-0285) (Fig. 1c), while cobalt nitrate results in the monoclinic $CoMoO_4$ phase (JCPDS No. 21-0868) (Fig. 1d). No obvious impurities could be detected from the XRD patterns.

The morphologies of the molybdates are observed by a scanning electron microscope (SEM). Fig. 2a is a SEM image of $Fe_2(MoO_4)_3$ product. The product mainly consists of sphere-like particles with average diameters of about 60 nm. The SEM image of $ZnMoO_4$ (Fig. 2b) shows plate-like structures. The plates are about 300 nm in diameter and 90 nm in thickness. The inset is a SEM image of a single particle, which clearly shows the plate morphology of the product. As shown

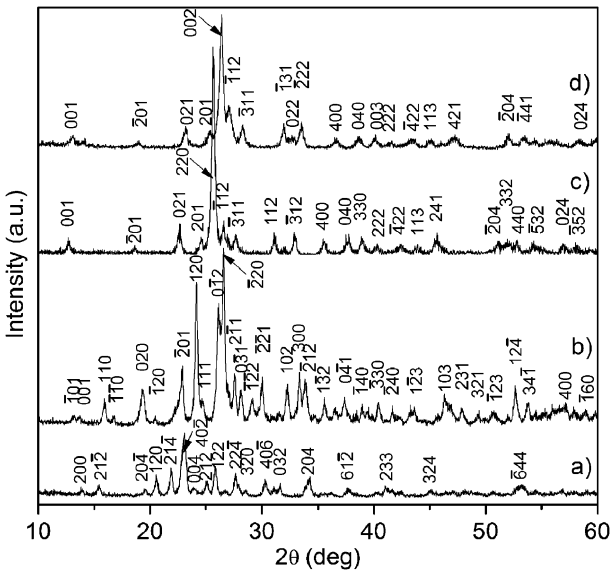

Fig. 1 XRD patterns of the as-synthesized molybdates, (a) $Fe_2(MoO_4)_3$, (b) $ZnMoO_4$, (c) $MnMoO_4$ and (d) $CoMoO_4$.

in Fig. 2c, the $MnMoO_4$ sample displays a rod-like morphology. The diameter of the rods ranges from tens to hundreds of nanometres and the length from hundreds of nanometres to several micrometres. The inset is a sectional view of the nanorods, revealing that some of the thin nanorods assemble into thick bundles. Fig. 2d gives a SEM image of the $CoMoO_4$ product, which shows nanowires with nearly uniform diameters of 70 nm. The lengths of the nanowires are up to hundreds of nanometres.

The morphological properties of the molybdates are further examined by a transmission electron microscope (TEM). Fig. 2e shows a typical TEM image of $Fe_2(MoO_4)_3$ nanoparticles. Unoverlapped particles are electron transparent and the average particle size is consistent with the result observed by SEM. Fig. 2f is the TEM image of the $ZnMoO_4$ nanoplates. It's noteworthy that obvious contrast change in a single nanoplate makes the nanoplates look coarse. Fig. 2g gives us a TEM view of $MnMoO_4$ nanorods. The rod-like morphology results are in exact accordance with SEM observations. Fig. 2h shows the TEM image of $CoMoO_4$ nanowires. In addition to $CoMoO_4$ nanowires, some tiny particles can also be found, which might be the fragments of nanowires produced in the heat-treatment process.

Taking $ZnMoO_4$ nanoplates as an example, the formation process can be described by the following reactions:

$$Mo_7O_{24}^{6-} + 8NH_3{\cdot}H_2O \rightarrow 7MoO_4^{2-} + 4H_2O + 8NH_4^{+} \quad (1)$$

$$Zn^{2+} + MoO_4^{2-} + nH_2O \rightarrow ZnMoO_4{\cdot}nH_2O \quad (2)$$

$$ZnMoO_4{\cdot}nH_2O \rightarrow ZnMoO_4 + nH_2O \quad (3)$$

After stirring the mixed solution for 2 h, $ZnMoO_4{\cdot}nH_2O$ is formed through the reaction between metal cations and MoO_4^{2-}, which are converted from $Mo_7O_{24}^{6-}$ in the presence of $NH_3{\cdot}H_2O$. To get a better understanding of the formation process, $ZnMoO_4{\cdot}nH_2O$ is characterized in detail by various techniques. SEM (ESI, Fig. S1†) and TEM images (Fig. 3a)

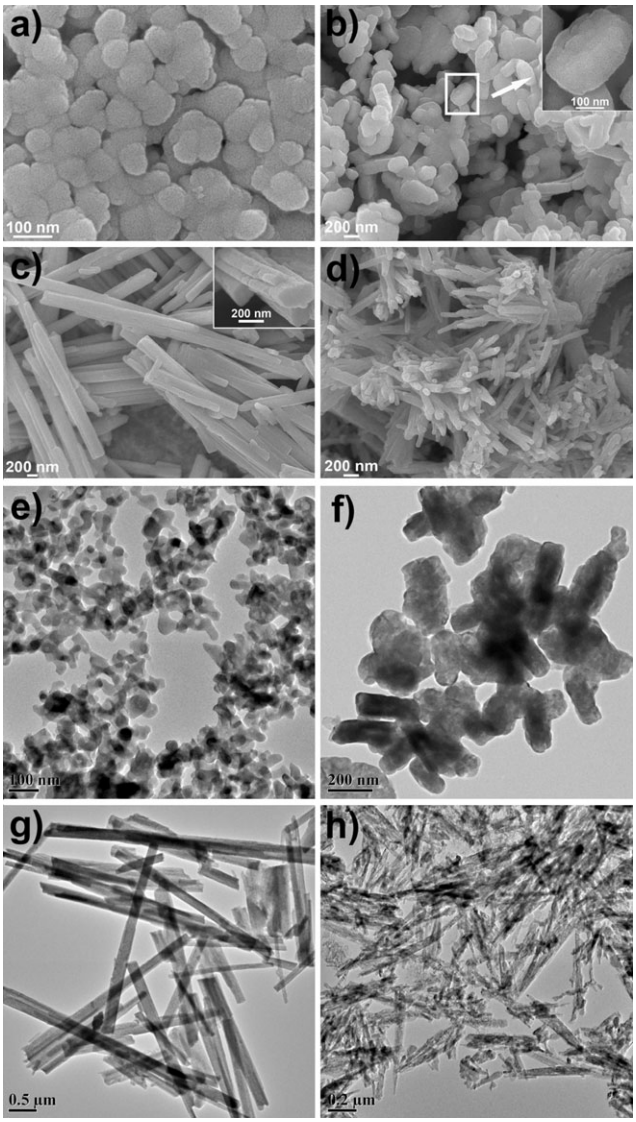

Fig. 2 SEM images of (a) $Fe_2(MoO_4)_3$, (b) $ZnMoO_4$, the inset is an SEM image of a single nanoplate, (c) $MnMoO_4$, the inset is a sectional view of the nanorods, (d) $CoMoO_4$, TEM images of (e) $Fe_2(MoO_4)_3$, (f) $ZnMoO_4$, (g) $MnMoO_4$ and (h) $CoMoO_4$.

illustrate that the hydrate has nearly the same particle size and shape as $ZnMoO_4$, demonstrating that no remarkable grain growth occurs in the heat-treatment process. The inset, the

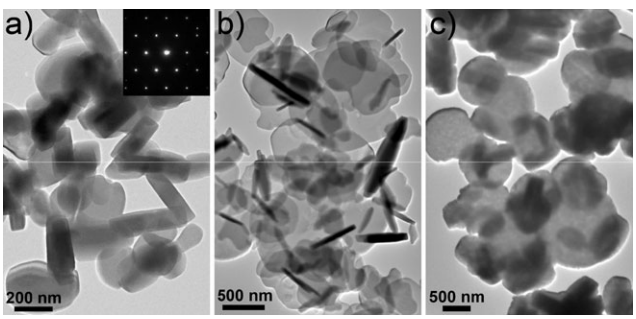

Fig. 3 TEM images of $ZnMoO_4{\cdot}nH_2O$ prepared with varied aging time, (a) 2 h, the inset is its SAED pattern, (b) 5 min and (c) 6 h.

selected area electron diffraction (SAED) pattern of the $ZnMoO_4{\cdot}nH_2O$ nanoplate, shows regular diffraction spots, indicating the single-crystal nature of the nanoplates.

The morphologies of $ZnMoO_4{\cdot}nH_2O$ can be affected by aging time. Fig. 3b and c show TEM images of $ZnMoO_4{\cdot}nH_2O$ aged for 5 min and 6 h, respectively. When the aging time is reduced to 5 min, the yield of product is very low. Thin slices with irregular shapes are obtained. The thickness is estimated to be 60 nm from the projection of erect slices. Whereas, when aging time is prolonged to 6 h, the particles become large, thick and to some extent agglomerated. Most of the irregular shapes disappear and the particles are mainly rounded. On the basis of these observations, it is reasonable to conclude that the formation of $ZnMoO_4{\cdot}nH_2O$ is a typical coarsening process. Coarsening, also named Ostwald ripening, is a widely observed phenomenon in crystal growth where large crystallites grow larger at the expense of small ones.[12]

The thermal behavior of $ZnMoO_4{\cdot}nH_2O$ is also examined by thermogravimetric analysis (TG) and differential thermal analysis (DTA) (ESI, Fig. S2†). There are only two apparent peaks in the range, corresponding to two weight loss steps. These two endothermic peaks centered at 105 °C and 272 °C can be explained as the two-step dehydration of $ZnMoO_4{\cdot}nH_2O$. There is no apparent endo- and exo-peak and no weight loss thereafter, thus the heat-treatment temperature is held at 400 °C, which is not enough to cause grain growth, as revealed by the above results. By comparison of the TEM images of $ZnMoO_4{\cdot}nH_2O$ and $ZnMoO_4$, it is noteworthy that $ZnMoO_4{\cdot}nH_2O$ nanoplates are smooth while $ZnMoO_4$ nanoplates look coarse for the contrast change in a single nanoplate. SAED patterns (ESI, Fig. S3†) also reveal that $ZnMoO_4$ nanoplates turn into polycrystal after heat-treatment. We think a lattice mismatch between $ZnMoO_4{\cdot}nH_2O$ and $ZnMoO_4$ is responsible for these changes. During the hydration, a mismatch between the lattices generates increasing strains. The difficulty of relieving these strains results in cracks and holes on the plates, which will appear as contrast change in TEM images. Meanwhile, the orientations of each part of the nanoplates become slightly different, which leads to the polycrystal nature of the $ZnMoO_4$ nanoplates.

A schematic diagram (Scheme 1) was proposed to illustrate the formation of $ZnMoO_4$ nanoplates. The formation process can be divided into three stages. At first, $ZnMoO_4{\cdot}nH_2O$ nuclei are formed *via* the reaction between Zn^{2+} and MoO_4^{2-} ions in the solution. After the initial nucleating process, large $ZnMoO_4{\cdot}nH_2O$ grains coarsen into nanoplates with the dissolution of small ones and separate from the solution. Finally, $ZnMoO_4$ nanoplates are obtained by heat-treating the $ZnMoO_4{\cdot}nH_2O$ precursor. Since the adopted experimental conditions are the same, we suggest the formation of all molybdates follows identical precipitation–coarsening–dehydration procedures. However, the morphologies of these molybdates differ very much from each other. In principle, final crystal morphologies depend on intrinsic crystal structure and reaction conditions.[13] In our experiments, the reaction conditions are the same. Thus, the difference between the molybdate hydrates in crystal structure is probably responsible for the varied morphologies.

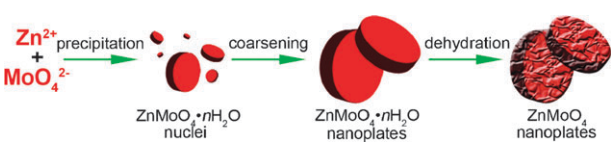

Scheme 1 Formation process of $ZnMoO_4$ nanoplates.

In conclusion, a general precipitation strategy has been developed for the large-scale synthesis of molybdate nanostructures. A series of molybdate nanostructures such as $Fe_2(MoO_4)_3$ nanoparticles, $ZnMoO_4$ nanoplates, $MnMoO_4$ nanorods and $CoMoO_4$ nanowires has been successfully prepared. This method provides a facile, low-cost and environment-friendly route for large-scale synthesis of molybdate nanostructures and might be expanded to synthesize many other molybdate nanocrystals, thus it might greatly facilitate the investigation and application of molybdates. This method may offer new opportunities for further investigation and application of molybdates. Further research on the performances of these molybdate nanocrystals is in progress.

This work was financially supported by the National Basic Research Program (2005CB623605) and Shanghai Nanotechnology Promotion Center (0552nm045).

Notes and references

1 (*a*) M. A. El-Sayed, *Acc. Chem. Res.*, 2004, **37**, 326–333; (*b*) C. N. R. Rao, G. U. Kulkarni, P. J. Thomas and P. P. Edwards, *Chem.–Eur. J.*, 2002, **8**, 29–35; (*c*) D. L. Leslie-Pelecky and R. D. Rieke, *Chem. Mater.*, 1996, **8**, 1770–1783; (*d*) E. Redel, R. Thomann and C. Janiak, *Chem. Commun.*, 2008, 1789–1791.

2 (*a*) A. Yu, N. Kumagai, Z. Liu and J. Y. Lee, *J. Power Sources*, 1998, **74**, 117–121; (*b*) A. E. Ovechkin, V. D. Ryzhikov, G. Tamulaitis and A. Zukauskas, *Phys. Status Solidi A*, 1987, **103**, 285–290; (*c*) A. S. Poghossian, H. V. Abovian, P. B. Avakian, S. H. Mkrtchian and V. M. Haroutunian, *Sens. Actuators, B*, 1991, **4**, 545–549.

3 (*a*) C. Mazzocchia, C. Aboumrad, C. Diagne, E. Tempesti, J. M. Herrmann and G. Thomas, *Catal. Lett.*, 1991, **10**, 181–191; (*b*) J. Kiwi, K. R. Thampi and M. Gratzel, *J. Chem. Soc., Chem. Commun.*, 1990, 1690–1692.

4 D. Spassky, S. Ivanov, I. Kitaeva, V. Kolobanov, V. Mikhailin, L. Ivleva and I. Voronina, *Phys. Status Solidi C*, 2005, **2**, 65–68.

5 H. Barry, F. Moore and D. Robitaille, *US Pat.*, 3 726 694, 1973.

6 (*a*) N. N. Leyzerovich, K. G. Bramnik, T. Buhrmester, H. Ehrenberg and H. Fuess, *J. Power Sources*, 2004, **127**, 76–84; (*b*) S. S. Kim, S. Ogura, H. Ikuta, Y. Uchimoto and M. Wakihara, *Chem. Lett.*, 2001, **30**, 760–761.

7 (*a*) V. B. Mikhailik, H. Kraus, D. Wahl and M. S. Mykhaylyk, *Phys. Status Solidi B*, 2005, **242**, R17–R19; (*b*) R. Sundaram and K. S. Nagaraja, *Sens. Actuators, B*, 2004, **101**, 353–360.

8 (*a*) A. M. Edwin Suresh Raj, C. Mallika, K. Swaminathan, O. M. Sreedharan and K. S. Nagaraja, *Sens. Actuators, B*, 2002, **81**, 229–236; (*b*) A. W. Sleight and B. L. Chamberland, *Inorg. Chem.*, 1968, **7**, 1672–1675; (*c*) A. P. Young and C. M. Schwartz, *Science*, 1963, **141**, 348–349.

9 (*a*) Y. Ding, S. H. Yu, C. Liu and Z. A. Zang, *Chem.–Eur. J.*, 2007, **13**, 746–753; (*b*) S. Lei, K. Tang, Q. Liu, Z. Fang, Q. Yang and H. Zheng, *J. Mater. Sci.*, 2006, **41**, 4737–4743.

10 F. Rullens, M. Devillers and A. Laschewsky, *J. Mater. Chem.*, 2004, **14**, 3421–3426.

11 F. Q. Dong and Q. S. Wu, *Appl. Phys. A: Mater. Sci. Process.*, 2008, **91**, 161–165.

12 (*a*) G. Oskam, Z. Hu, R. L. Penn, N. Pesika and P. C. Searson, *Phys. Rev. E: Stat., Nonlinear, Soft Matter Phys.*, 2002, **66**, 011403; (*b*) P. Y. Silvert, R. Herrera-Urbina and K. Tekaia-Elhsissen, *J. Mater. Chem.*, 1997, **7**, 293–299.

13 (*a*) S. M. Lee, S. N. Cho and J. Cheon, *Adv. Mater.*, 2003, **15**, 441–444; (*b*) X. B. Cao, X. M. Lan, C. Zhao, W. J. Shen, D. Yao and W. J. Gao, *J. Cryst. Growth*, 2007, **306**, 225–232.